W&M ScholarWorks

2017

Late-summer biogeochemistry in the Mertz Polynya: East Antarctica

E. H. Shadwick
Virginia Institute of Marine Science

B. Tilbrook
University of Tasmania

K. I. Currie
University of Otago

RESEARCH ARTICLE

Key Points:
- Enhanced net community production persists 3 years after Mertz Glacier calving
- New polynya configuration appears to favor enhanced surface ocean CO_2 uptake
- Surface CO_2 undersaturation in the eastern shelf and slope appears supported by input of residual or excess alkalinity from melting sea ice

Correspondence to:
E. H. Shadwick,
shadwick@vims.edu

Late-summer biogeochemistry in the Mertz Polynya: East Antarctica

E. H. Shadwick[1,2] [ID], B. Tilbrook[2,3] [ID], and K. I. Currie[4] [ID]

[1]Virginia Institute of Marine Science, College of William & Mary, Gloucester Point, Virginia, USA, [2]Antarctic Climate & Ecosystems Cooperative Research Centre, University of Tasmania, Hobart, Tasmania, Australia, [3]CSIRO Oceans and Atmosphere, Hobart, Tasmania, Australia, [4]Centre for Chemical and Physical Oceanography, National Institute of Water and Atmospheric Research, University of Otago, Dunedin, New Zealand

Abstract A marked reconfiguration of the Mertz Polynya following the 2010 calving of the Mertz Glacier Tongue has been associated with a decrease in the size and activity of the polynya. We report observations of the oceanic carbonate (CO_2) system in late-summer 2013, the third post-calving summer season. Estimates of seasonal net community production (NCP) based on inorganic carbon deficits and the oxygen-argon ratio indicate that the waters on the shelf to the east of Commonwealth Bay (adjacent to the Mertz Glacier) remain productive compared to pre-calving conditions. The input of residual or excess alkalinity from melting sea ice is found to contribute to the seasonal enhancement of carbonate saturation state and pH in shelf waters. Mean rates of NCP in 2012–2013 are more than twice as large as those observed in the pre-calving summers of 2001 and 2008 and suggest that the new (post-calving) configuration of the polynya favors enhanced net community production and a stronger surface ocean sink for atmospheric CO_2 due at least in part to the redistribution of sea ice and associated changes in summer surface stratification.

1. Introduction

Coastal polynyas, areas of open water within the sea ice, play a role in air-sea gas exchange [*Yager et al.*, 1995; *Sweeney et al.*, 2000; *Else et al.*, 2012], sea ice and dense water formation [*Orsi et al.*, 1999; *Williams and Bindoff*, 2003; *Tamura et al.*, 2012], and primary production [*Arrigo and van Dijken*, 2003; *Shadwick et al.*, 2013a]. Coastal polynyas form where strong katabatic winds drive recently formed sea ice away from the coast, or another barrier such as a floating glacier tongue. Polynyas produce and export large quantities of sea ice and brine released during the formation of this ice increases the salinity and density of the underlying surface waters. Large volumes of dense shelf water, the precursor to Antarctic Bottom Water (AABW) are produced in Antarctic coastal polynyas [*Rintoul*, 1998; *Orsi et al.*, 1999]. In the Southern Ocean, the primary sources of dense shelf water come from the Weddell Sea, the Ross Sea, and the East Antarctic polynyas near the Mertz Glacier and surrounding embayments, collectively referred to as the Mertz Polynya [*Orsi et al.*, 1999].

Polynya surface waters are often the first areas of the polar regions to be exposed to solar radiation with the return of the springtime sun, either due to reduced or absent ice cover, or because they often experience early break out of ice in spring [*Mundy and Barber*, 2001; *Shadwick et al.*, 2011]. Both Arctic [*Miller et al.*, 2002; *Shadwick et al.*, 2011] and Antarctic [*Smith and Gordon*, 1997; *Arrigo and van Dijken*, 2003] coastal polynyas are thus often associated with high rates of spring and summer primary production. Relationships between polynya dynamics and primary production have been reported in both Arctic [*Arrigo and van Dijken*, 2004] and Antarctic systems [*Arrigo and van Dijken*, 2003; *Cape et al.*, 2014], with the timing of ice melt and the onset of summer stratification influencing the intensity of phytoplankton blooms and associated air-sea CO_2 disequilibrium. Furthermore, the recent collapse of the Larsen ice shelves has been associated with newly uncovered embayments hosting seasonal production of similar magnitude to Antarctic coastal polynyas [*Cape et al.*, 2014]. The Mertz Polynya system in East Antarctica is of considerable interest following dramatic changes to the polynya dynamics and biogeochemical system after the 2010 calving of the Mertz Glacier Tongue [*Tamura et al.*, 2012; *Shadwick et al.*, 2013a; *Nihashi and Ohshima*, 2015; *Ohshima et al.*, 2016].
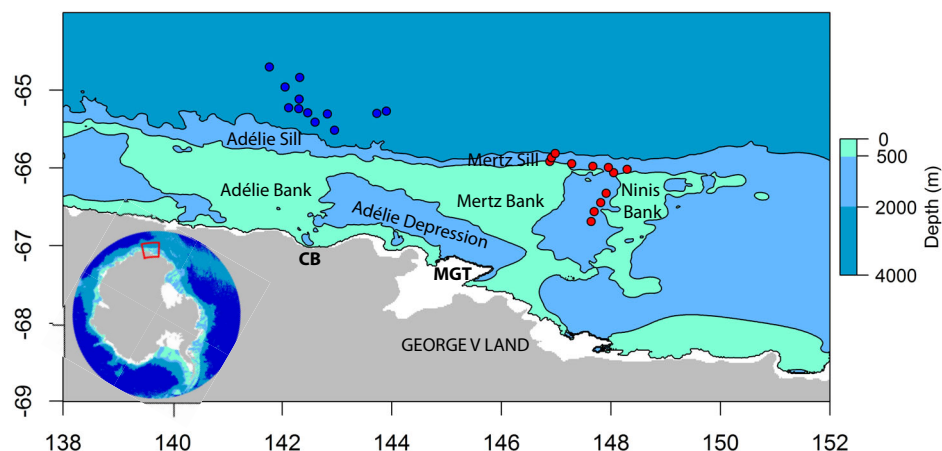
Figure 1. Map of the study area in the George V Land region of East Antarctica. Major features, including the Adélie Sill, Adélie Bank, Adélie Depression, Mertz Bank, Mertz Sill, Ninis Bank, the Mertz Glacier Tongue (MGT), and Commonwealth Bay (CB) are indicated. The locations of stations occupied in February 2013 offshore from the Adélie Sill are in blue and those on the shelf are in red.

Prior to 2010, the existence of the coastal Mertz Polynya could be attributed primarily to two environmental factors. First, the floating Mertz Glacier Tongue (MGT) acted as a barrier to the westward advection of sea ice associated with the Antarctic Coastal Current. Second, katabatic winds drove the formation of sea ice, particularly in the lee of the MGT, and subsequently pushed the sea ice offshore [*Massom et al*., 1998]. The icescape in the Mertz Polynya has undergone significant recent changes, largely precipitated by the February 2010 ungrounding of iceberg B09b [*Young et al*., 2010], and the subsequent calving of the Mertz Glacier Tongue (Figure 1) [*Shadwick et al*., 2013a]. Prior to the MGT calving, the Mertz Polynya was one of the largest in East Antarctica in terms of sea ice production [*Tamura et al*., 2008, 2012]. In 2011, the first summer after the MGT calving, the size of the polynya was reduced and sea ice production declined substantially [*Tamura et al*., 2012; *Shadwick et al*., 2013a]. A significant freshening of the surface waters and dense shelf waters in the summer of 2011 has been reported [*Shadwick et al*., 2013a]. A recent estimate indicates that the amount of sea ice production in the Mertz Polynya following the MGT calving decreased by as much as 40%, repositioning the region as the fifth largest polynya with respect to Antarctic sea ice production [*Nihashi and Ohshima*, 2015; *Ohshima et al*., 2016].

Following the MGT calving, several large sections of iceberg B09b remain grounded in Commonwealth Bay; the iceberg has restricted the offshore transport of ice and imposed a near year-round sea ice coverage of Commonwealth Bay. By contrast, the region east of Commonwealth Bay has a larger area of open water relative to the pre-MGT calving configuration due to the absence of both the MGT and the large area of fast-ice that had previously built up east of the glacier tongue. We report observations from late-summer 2013 that suggest the region remains in a state of transition. Summer mixed-layer depths remain shallow relative to the pre-calving conditions and the biogeochemical response to the physical environmental changes appears to have persisted in shelf waters through three summer seasons.

2. Methods

The primary data sets were collected on board the New Zealand National Institute of Water and Atmospheric Research (NIWA) R/V Tangaroa between 2 February and 12 March 2013 at stations shown in Figure 1 as part of a joint New Zealand-Australia research cruise (TAN1302) [*Williams*, 2013]. Additional observations from earlier voyages on board the Australian R/V Aurora Australis in January 2008 (AU0803) [*Rosenberg and Rintoul*, 2010], January 2011 (AU1121) [*Rosenberg and Rintoul*, 2011], and January 2012 (AU11203) [*Rosenberg and Rintoul*, 2012] are also presented to give a broader context for the recent changes in the region (Figure 2).

On the 2013 voyage, data were acquired using a Seabird SBE9plus, with dual temperature and conductivity sensors mounted on a SeaBird 24 bottle rosette frame with 22 Ocean Test Equipment 10 L bottles. The
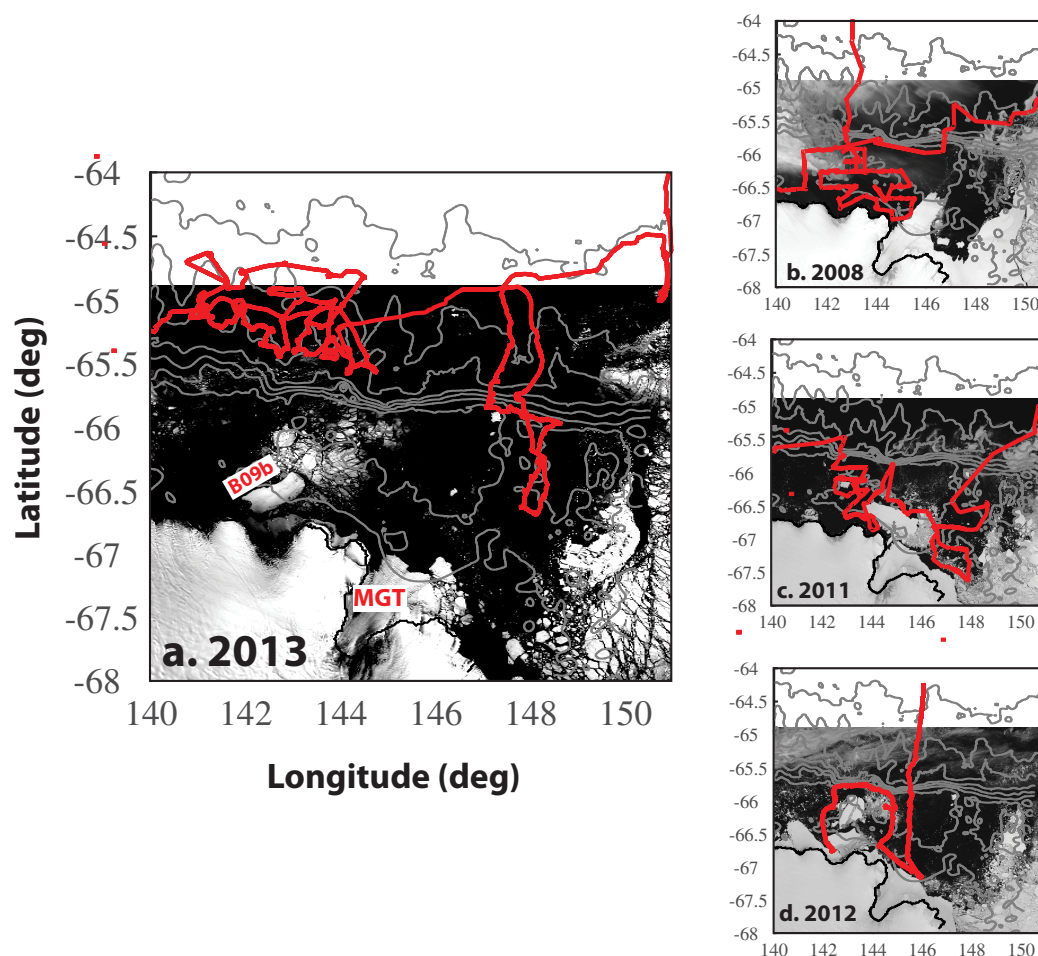
Figure 2. (a) Cruise track of the R/V Tangaroa during the joint New Zealand-Australia voyage in summer 2013 is overlaid on a Rapid Response MODIS image from the NASA's EarthData portal (www.earthdata.nasa.gov). The Mertz Glacier Tongue (MGT) and iceberg B09b are indicated; (right) the cruise tracks and sea-ice conditions of previous voyages on board the R/V Aurora Australis in January (b) 2008, (c) 2011, and (d) 2012.

accuracy of temperature and salinity data were ∼0.001°C, and ∼0.003 kg m^{-3}, respectively. On the earlier voyages, data were collected using a SeaBird SBE9plus CTD, with dual temperature and conductivity sensors mounted on a SeaBird 24 bottle rosette frame, with 22 General Oceanics 10 L Niskin bottles. The accuracy of temperature and salinity data from the RV Aurora Australis voyages (in 2008, 2011, and 2012) were ∼0.001°C, and ∼0.002 kg m^{-3}, respectively.

2.1. Biogeochemical Observations

Discrete measurements of dissolved inorganic carbon (TCO_2) and total alkalinity (AT) were made by coulo-metric (using a SOMMA system) and (open cell) potentiometric titration (using components from Metrohm), respectively [*Dickson et al.*, 2007]. The AT analyses of samples from the 2013 cruise were made on board the RV Tangaroa; TCO_2 samples from the same cruise were fixed with a solution of mercuric chloride ($HgCl_2$), and stored in the dark at 4°C before analysis in the laboratory at CSIRO in Hobart after the voyage. Samples from the 2008, 2011, and 2012 voyages were analyzed on board the RV Aurora Australis. Regular analysis of Certified Reference Materials (provided by A. G. Dickson, Scripps Institution of Oceanography) ensured that the uncertainty (accuracy and precision) of the all the TCO_2 and AT measurements presented was better than 2.1 μmol kg^{-1} for both parameters. Using the standard set of carbonate system equations pH (on the seawater scale) and aragonite saturation state (Ω) were computed using the CO2SYS program of *Lewis and Wallace* [1998] and using the equilibrium constants of *Mehrbach et al.* [1973] refit by *Dickson and Millero* [1987]. The calcium (Ca^{2+}) concentration was assumed to be conservative and calculated as a function of salinity [*Riley and Tongudai*, 1967]. Nitrate (NO_3^-) plus nitrite (NO_2^-), hereafter "nitrate," was measured
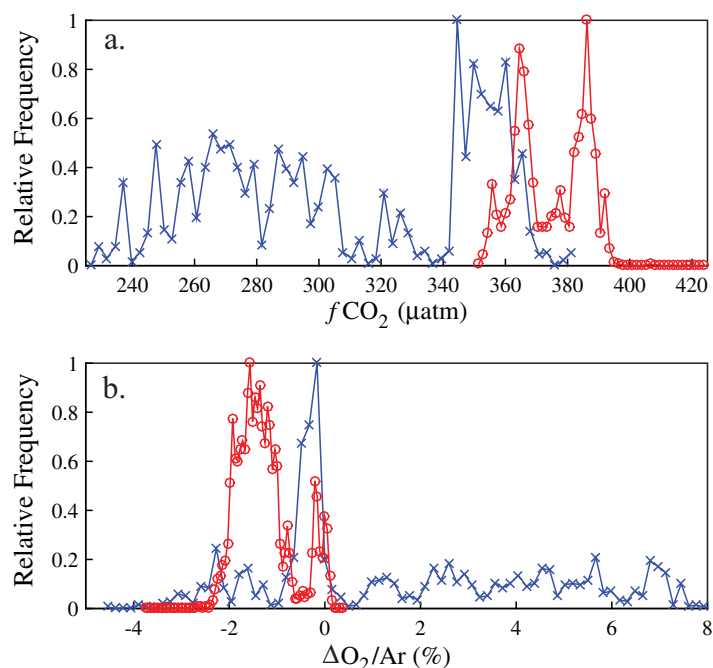
Figure 3. Frequency distributions of (a) fCO_2 and (b) $\Delta O_2/Ar$ in the survey region, with 2013 observations in waters north of the slope in blue, and over the shelf in red. All frequencies have been normalized to a maximum value of 1 to facilitate comparison between the two plots.

following standard procedures [*Grasshoff et al.*, 2007], including use of gravimetric nitrate standards prepared at sea, and has associated uncertainty (accuracy and precision) of 0.03 μmol L^{-1}.

2.2. Underway fCO_2 and O_2/Ar Measurements

Observations of surface CO_2 fugacity (fCO_2) and the ratio between oxygen and argon (O_2/Ar) were made along the cruise track using the ship's underway seawater supply (Figure 3). Surface water fCO_2 from an intake roughly 5.5 m below the surface was measured by continuous flow equilibration (General Oceanics Inc., model 8050) [*Pierrot et al.*, 2009], via a nondispersive infrared spectrometer (LiCor, LI7000). The system was calibrated every 4 h with four standards: a CO_2-free air, and three concentrations of CO_2 (332.98, 394.49, and 425.15 ppm) in dry air on the WMO-X2007 mole fraction scale. The fCO_2 data were corrected to in situ water temperature and to 100% humidity following *Pierrot et al.* [2009] and have an uncertainty of less than ± 2 μatm based on field comparisons [*Körtzinger et al.*, 2000].

The ratio of dissolved oxygen and argon (O_2/Ar) was measured using a Pfeifer QMS200 quadrupole mass spectrometer and equilibrator inlet [*Cassar et al.*, 2009] with water from the same supply as the CO_2 system. The travel time between the intake and the CO_2 and O_2/Ar systems is less than 3 min, and warming is typically less than 0.5°C.

2.3. Air-Sea CO_2 Flux Computations

The air-sea CO_2 flux was computed using the following equation:

$$F = k\alpha\Delta fCO_2, \tag{1}$$

where F is the flux (mmol m^{-2} d^{-1}), k and α are the gas transfer coefficient and coefficient of solubility [*Weiss*, 1974], respectively, and ΔfCO_2 is the gradient in CO_2 between the ocean and the atmosphere. The gas transfer term was computed from the NCEP/NCAR wind speed reanalysis product [*Kalnay et al.*, 1996] and the parameterization of *Wanninkhof* [2014].

2.4. Partitioning of Seasonal Changes in TCO_2

Seasonal depletions in mixed-layer TCO_2 were estimated from the difference between (observed) summer concentrations and an inferred winter concentration. For stations located to the north of the Adélie Sill (see Figure 1, in blue), the winter concentrations were estimated from the observed TCO_2 concentrations at the depth of the temperature minimum [e.g., *Ishii et al.*, 2002; *Jones et al.*, 2011]. Because the temperature minimum is not as well defined on the shelf, this method of defining the winter concentration may not be appropriate in the marginal ice zone, where some of our stations are located [e.g., *Shadwick et al.*, 2013a]. For our shelf stations, we therefore defined the winter TCO_2 concentration by the observed value at a depth of 150 m in shelf waters (mean of 2220 μmol kg^{-1}, standard deviation of 5 μmol kg^{-1}; see Figure 1, in red) following *Shadwick et al.* [2014]; winter mixing on the shelf extends well below this depth [e.g., *Williams and*

Bindoff, 2003]. The winter TCO_2 concentration for the slope stations was defined by the value at the temperature minimum (mean of 2225 μmol kg^{-1}, standard deviation of 12 μmol kg^{-1}).

The TCO_2 deficits result from the influence of both physical and biological processes: air-sea CO_2 exchange, mixing, photosynthesis and respiration, and the formation and dissolution of calcium carbonate all impact surface deficits. The total deficit in TCO_2 can be expressed as the sum of the contributing processes:

$$\Delta TCO_2^{total} = \Delta TCO_2^{sal} + \Delta TCO_2^{alk} + \Delta TCO_2^{bio+gas}. \quad (2)$$

The "total" deficit is integrated difference between observed summer and inferred winter concentrations in the upper 100 m. The "sal" deficit is determined from the difference between observed and salinity-normalized TCO_2, where salinity normalization was done with an inferred winter salinity at 150 m for the shelf stations (34.35), and at the temperature minimum for the slope stations (34.45). We assume that this term accounts for changes in TCO_2 resulting from mixing with water masses of different salinity whether these are due to horizontal and/or vertical processes. The "alk" term refers to the impact of carbonate mineral formation or dissolution on TCO_2. Because the precipitation or dissolution of $CaCO_3$ results in a 2:1 change in TA:TCO_2, we estimate the "alk" term based on the AT deficit, after accounting for changes in salinity and nitrate [e.g., *Jones et al.*, 2011]. The remaining "bio + gas" term represents changes due to biological processes and gas exchange and are grouped together.

2.5. Net Community Production Computations

The rate of net community production (NCP, the imbalance between net primary production and heterotrophic respiration) was estimated from underway measurements of O_2/Ar. By assuming steady state and neglecting vertical mixing, NCP was estimated via:

$$NCP \sim k_{O_2}[O_2]_{sat}\Delta(O_2/Ar), \quad (3)$$

where k_{O_2} is the gas exchange velocity for oxygen, $[O_2]_{sat}$ is the O_2 concentration at saturation, and $\Delta(O_2/Ar)$ is the biologically mediated change in oxygen [*Cassar et al.*, 2007]. Wind speed from the NCEP/NCAR wind speed reanalysis product [*Kalnay et al.*, 1996] and the parameterization of *Wanninkhof* [2014] for long-term winds were used to compute k_{O_2}. The weighting method of *Reuer et al.* [2007] was used to account for the wind speed history prior to the arrival of the ship on station. The net organic carbon production was determined from the oxygen derived NCP, using a photosynthetic quotient of 1.4 [*Laws*, 1991; *Bender et al.*, 1999]. The use of the O_2/Ar-based estimated of NCP in high latitude regions is complicated by a number of processes including: short-term temperature changes, ice melt, and the entrainment of oxygen-poor subsurface waters [e.g., *Castro-Morales et al.*, 2013; *Cassar et al.*, 2014; *Eveleth et al.*, 2014; *Shadwick et al.*, 2015]. In particular, the entrainment of O_2-poor water from below the surface would tend to underestimate NCP [*Cassar et al.*, 2014], and the NCP estimates using this method should therefore be considered minimum values. The method nevertheless provides an alternative, shorter-term view of NCP compared to the conventional seasonal carbon or nitrate deficit approaches described below.

An independent estimate of NCP was made from depth integrated (0–100 m) deficits of salinity-normalized TCO_2 (see previous section; the depth integration accounts for potential vertical redistribution of TCO_2 due to changes in mixed-layer depth over the productive season [e.g., *Bates et al.*, 1998]. The length of the productive season was defined as 60 days for the 2008, 2011, and 2012 data (collected in January) and 90 days for the 2013 data (collected in February), based on an onset of primary production inferred from MODIS chl *a* concentration (via the Oregon State University Ocean Productivity website).

The different time scales of the two methods hinder a direct comparison: the O_2/Ar method integrates over the length of time required to exchange oxygen between the mixed-layer and atmosphere (days to weeks), while the TCO_2 based estimate integrates over a number of months between the observations and the previous winter (i.e., over the entire productive season). However, because the brief period of open water productivity dominates the seasonal cycle in this, and other high latitude systems [e.g., *Roden et al.*, 2013; *Legge et al.*, 2017], the bias between the two methods is likely limited.
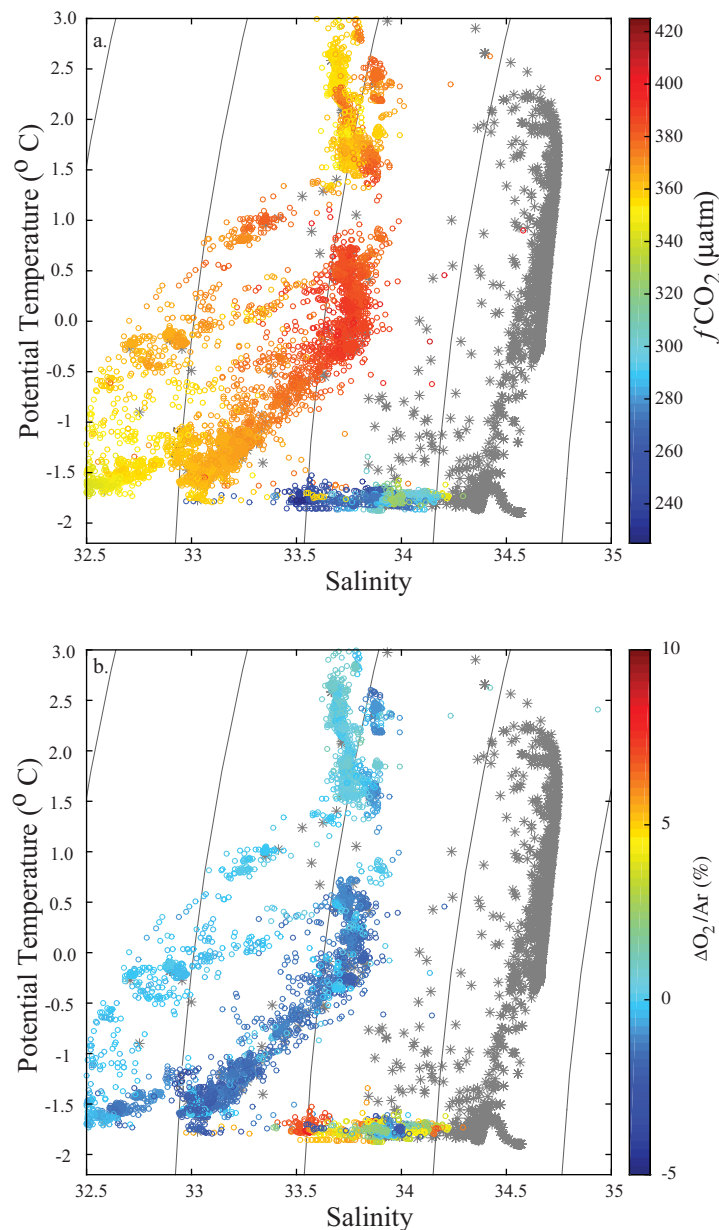
Figure 4. Surface (a) fCO$_2$ and (b) ΔO$_2$/Ar as a function of temperature and salinity in 2013. Grey symbols correspond to subsurface data without associated underway observations.

3. Results

3.1. Hydrographic Properties

The surface waters in the study region were relatively cool and fresh (Figures 4 and 5), with salinities ranging from roughly 32.5 to 34.2 and temperature generally below 1.5°C but reaching a maximum 3°C, and consistent with Antarctic Surface Waters previously observed in this region [Shadwick et al., 2014]. While the observations presented here were collected on the shelf, and in waters north of the continental slope, we refer to two broad regions, "shelf" defined as the region south of 66.2°S and east of 146.9°E, and "slope" defined as the region north 66.2°S, and further partitioned into slope waters north of the Adélie Sill (west of 145°E) and north of the Mertz Sill (east of 147°E) for analysis of surface water properties in this and the subsequent section (Figure 1).

Relatively cool, salty waters were observed on the shelf, and at the southern edge of the slope region north of the Adélie Sill. On the shelf, where sea-ice formation has long been associated with the lee of the Mertz Glacier and the Mertz Polynya, surface waters were roughly −1.8°C with a maximum surface salinity exceeding 34 (Figures 5a and 5b). In the northernmost slope region waters with temperatures > 0°C, likely resulting from the onshore intrusion of warm, saline, modified Circumpolar Deep Water (mCDW) were observed. There is a longitudinal gradient in the surface properties of the slope waters with the most saline waters observed between 140°E and 144°E north of the Adélie Sill, while the slope waters to the east (north of the Mertz Sill) were associated with a regional surface salinity minima. A similar pattern in temperature was evident with the waters over the slope region north of the Adélie Sill generally warmer than 0°C, with much cooler surface waters observed north of the Mertz Sill (Figure 5).

The subsurface water properties indicate the presence of mCDW as well as modified shelf water (mSW). The mSW results from mixing between dense shelf water (DSW), characterized by near-freezing temperatures and salinity greater than 34.4 (Figures 4 and 6) and formed during sea ice formation, and mCDW. This mixing occurs in transit from the shelf to the slope. Previous work in this region has shown that the DSW
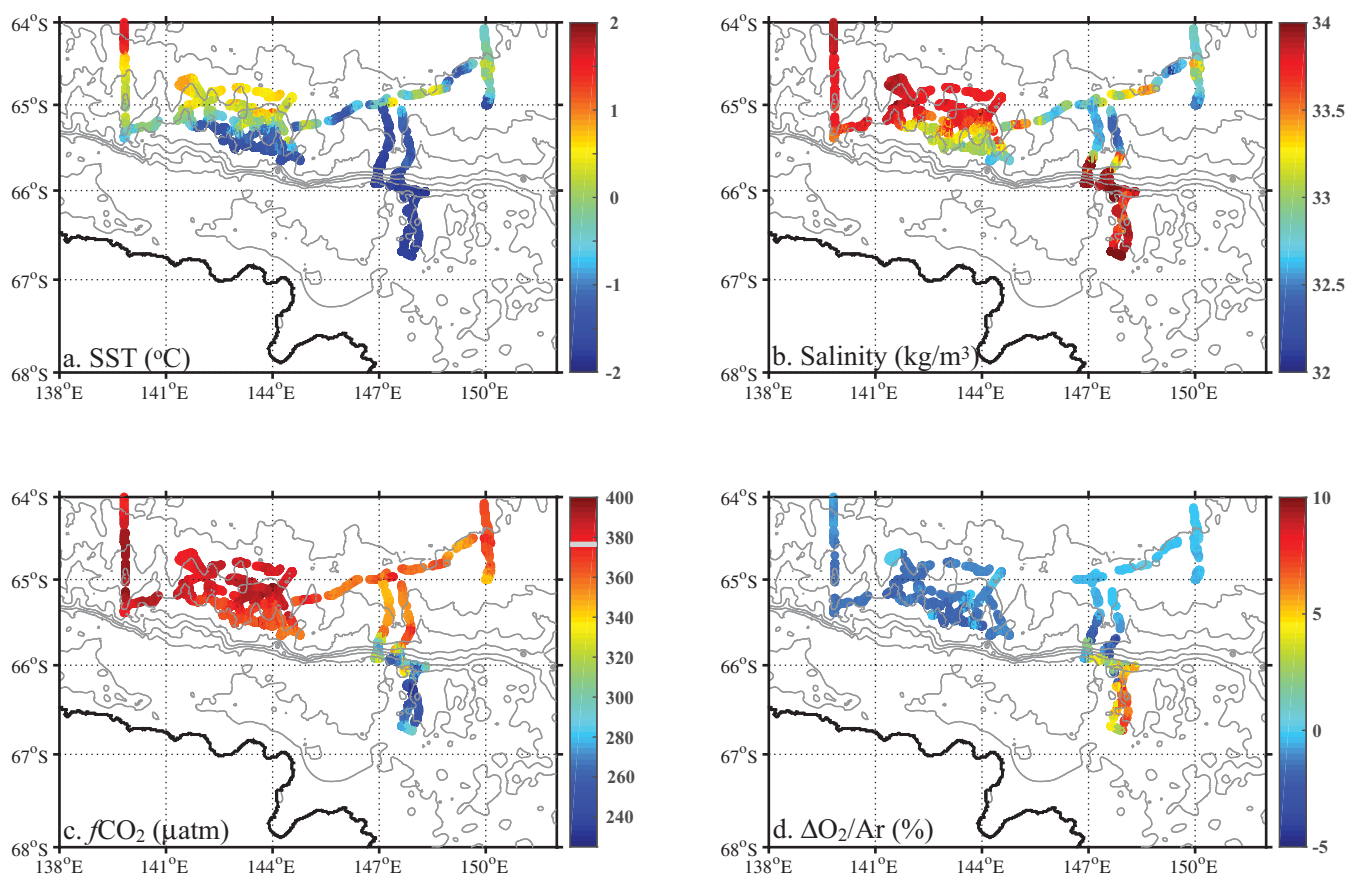
Figure 5. Spatial distribution of (a) sea-surface temperature (SST), (b) salinity, (c) fCO$_2$, and (d) ΔO$_2$/Ar in 2013 in the survey region. The mean atmospheric fCO$_2$ (378 μatm) is indicated by the grey horizontal line on the color bar in Figure 5c for reference.

undergoes a biological modification on the shelf, and the outflowing mSW (which is a mixture of DSW and mCDW) is depleted in TCO$_2$ relative to inflowing CDW and mCDW [*Shadwick et al.*, 2014]; the late-summer observations presented here are consistent with this view.

3.2. Biogeochemical Surface Properties

The surface waters exhibit a distinct change in biogeochemical properties between the shelf and slope regions. The underway data indicate that the high salinity and low temperature waters found on the shelf, were associated with minimum values of fCO$_2$ (Figure 5c), and maximum values of O$_2$/Ar (Figure 5d). Waters over the slope were associated with somewhat higher fCO$_2$ and near zero, or negative values of O$_2$/Ar. The majority of the observations indicate supersaturation with respect to atmospheric CO$_2$, with values in the slope region ranging from near equilibrium ($\sim$390 μatm) north of the Mertz Sill in the east, to roughly 400 μatm at the northern edge. Consistent with the longitudinal gradient in hydrography, the surface waters in the slope region north of the Adélie Sill indicate maximum fCO$_2$ near 140°E and decrease to undersaturated values (350–380 μatm) in waters north of the Mertz Sill. By contrast the waters on the shelf indicate an undersaturation of more than 100 μatm, with values as low as 230 μatm.

The O$_2$/Ar observations indicate a similar spatial pattern with maximum values ($\sim$10% supersaturation), indicating a net biological production of oxygen, or photosynthesis associated with regions of low fCO$_2$ on the shelf. By contrast the slope waters indicate values of net biological oxygen consumption, or respiration ($\sim$5% undersaturation) in regions of maximum fCO$_2$, and near neutral, or zero values of O$_2$/Ar where the fCO$_2$ is roughly in equilibrium with the atmosphere in the slope region north of the Mertz Sill. The O$_2$/Ar observations alone do not allow us to attribute all negative signals to net respiration, or heterotrophy, due to the influence of mixing. The correlation between elevated fCO$_2$ and negative values of O$_2$/Ar in the
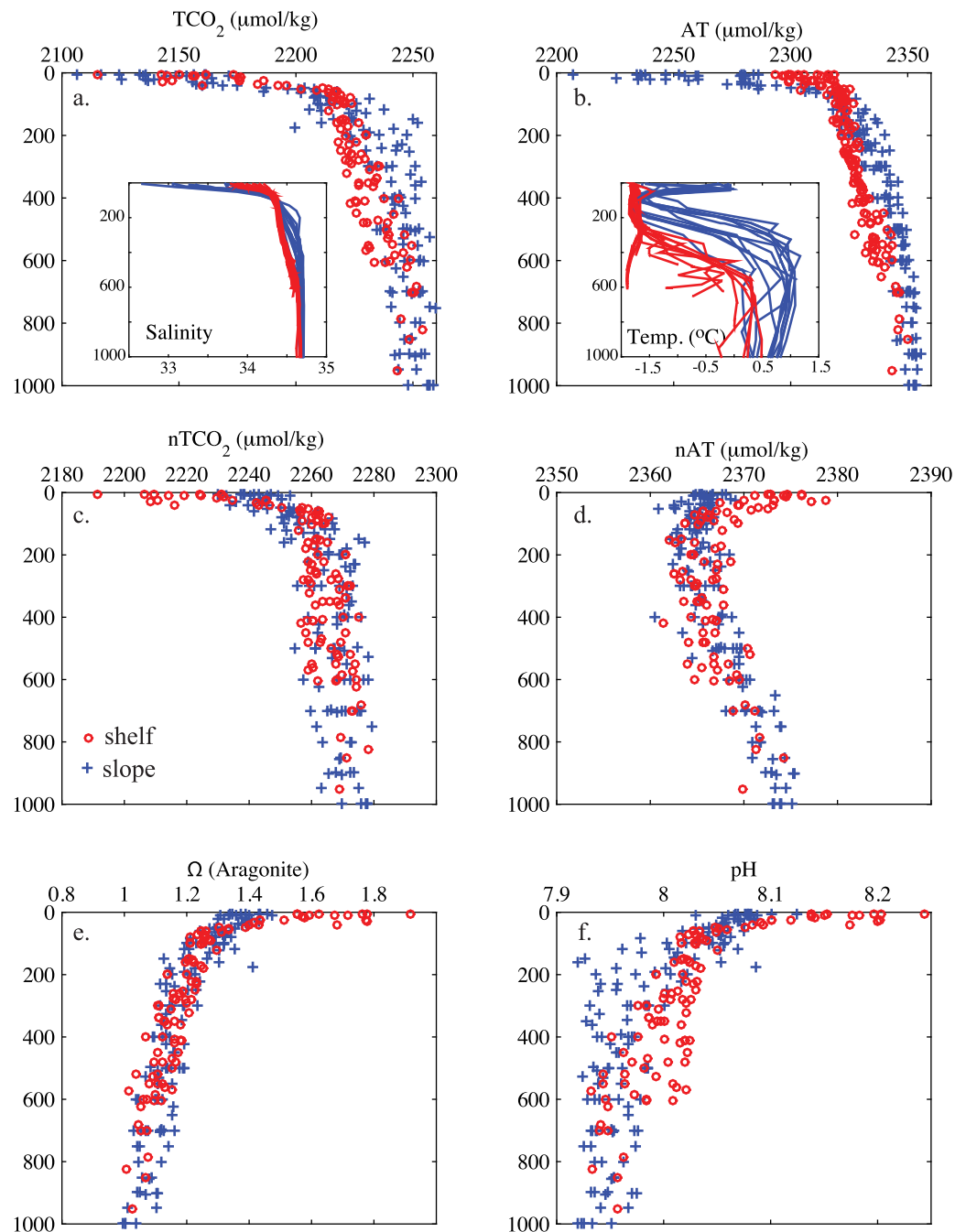
Figure 6. Upper ocean profiles of CO_2 system parameters in slope (blue) and shelf (red) waters collected in 2013. (a) TCO_2 with salinity inset; (b) AT with temperature inset; (c) salinity-normalized TCO_2 ($nTCO_2$); (d) salinity-normalized AT (nAT); (e) aragonite saturation state (Ω); and (f) pH (on the seawater scale).

surface waters of the slope region north of the Adélie Sill, is likely a result of both local respiration in the surface waters as well as the upward mixing of warm, saline, O_2-poor and CO_2-rich mCDW.

Wind speeds were fairly consistent throughout the period of observation (5–9 m/s) and we observed CO_2 uptake in the surface waters over the shelf and outgassing in surface waters over the slope. Like the O_2/Ar observations, the spatial variation in the air-sea CO_2 flux results from both physical and biological processes. While there was ice present in the region at the time of observation (see Figure 2a), we have not attempted to scale the fluxes presented here by the degree of ice cover, nor to integrate them to yield annual values, but rather consider the estimates representative of the fluxes during the mostly open water, summer
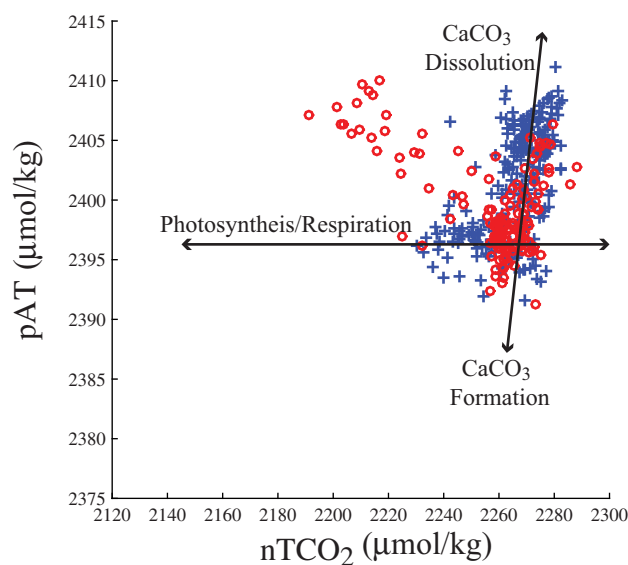
Figure 7. The relationship between potential alkalinity (pAT) and salinity-normalized TCO_2, with the impact of $CaCO_3$ formation and dissolution, and photosynthesis/respiration indicated schematically. Observations are from 2013.

season. Fluxes in the shelf region were dominated by significant uptake ranging from -30 to -5 mmol C m^{-2} d^{-1}. In the slope region north of the Adélie Sill, there was modest uptake ($\sim$5 mmol C m^{-2} d^{-1}) at the southern edge, and a transition to outgassing of up to 10 mmol C m^{-2} d^{-1} further offshore. By contrast, the slope waters north of the Mertz Sill indicate modest uptake of atmospheric CO_2 with fluxes on the order of -5 to -10 mmol C^{-2} d^{-1}.

3.3. CO$_2$ System Properties

Profiles of TCO_2 indicate near surface depletions in both the shelf and slope regions, with roughly the same surface to deep gradient (Figure 6a); the surface deficit results from a combination of freshwater input from seasonal ice melt, air-sea exchange, biological processes and the formation and dissolution of carbonate minerals (see also section 2.4). The near surface AT concentrations are more spatially distinct, with values in the slope region up to 100 μmol kg^{-1} lower than in the shelf waters (Figure 6b). Subsurface concentrations indicate modest differences in TCO_2 and AT between regions, with the slope waters showing elevated concentrations relative to the shelf region in 200–600 m depth range that is associated with elevated salinity for slope waters and temperatures between 0.5 and 1°C. The subsurface concentrations of TCO_2 and AT are consistent with the characteristic concentrations of CDW, mCDW, and mSW previously reported for this region [*Shadwick et al.*, 2014] as well as those found elsewhere in East Antarctica [*Roden et al.*, 2016].

Normalizing to a constant salinity removes the effect of variable salinity on TCO_2 and AT concentrations (Figures 6c and 6d). In the shelf region concentrations of $nTCO_2$ were between 20 and 50 μmol kg^{-1} less than mixed-layer concentrations in the slope region, while the subsurface concentrations of $nTCO_2$ are similar and range from 2250 to 2280 μmol kg^{-1}. The opposite is seen in the nAT profiles: the near surface concentrations on the shelf were roughly 10 μmol kg^{-1} higher than those on the slope. The subsurface concentrations of $nTCO_2$ in both regions ranged from 2250 to 2280 μmol kg^{-1}; subsurface nAT was similarly consistent between regions with values between 2365 and 2375 μmol kg^{-1}.

Both the carbonate saturation state and the pH, computed from observations of TCO_2 and AT, reflect differences in surface concentrations described above (Figures 6e and 6f). While the $nTCO_2$ in the surface waters on the shelf was more depleted than in waters on the slope, the nAT in shelf waters was also elevated. Both the drawdown of TCO_2 (via conversion of CO_2 to organic matter during photosynthesis) and the production of AT (potentially via dissolution of carbonate minerals in melting sea ice) contribute to enhanced saturation states (1.6–1.8) observed in the surface waters on the shelf, which are influenced by the input of melting sea ice in summer. This is in contrast to the weaker surface $nTCO_2$ depletion and the absence of enhanced surface nAT in the slope regions, resulting in surface saturation states of roughly 1.4. A similar enhancement of surface pH (8.2) resulting from both the depletion of surface water TCO_2 and the additional AT is observed in the shelf region, in contrast to the slope region which had surface pH of roughly 8.1.

It has been shown that TCO_2 may be more efficiently rejected than AT with brine during sea ice formation, and that this may result in ratios of TCO_2:AT in sea ice that differ from those in the underlying seawater [*Rysgaard et al.*, 2007; *Geilfus et al.*, 2012]. Several studies in both Arctic and Antarctic sea ice using both observations [e.g., *Dieckmann et al.*, 2008; *Geilfus et al.*, 2012] and models [*Moreau et al.*, 2016] have shown that carbonate mineral precipitation may have important implications for the AT concentration of the underlying seawater and consequences for the so called sea ice carbonate pump. Earlier work in the Mertz Polynya

region suggested that carbonate mineral processes did not significantly influence AT concentrations on the shelf [*Shadwick et al.*, 2014]; the present late-summer observations indicate that there may be a source of AT to the surface waters on the shelf. Once corrected for the influence of changes in salinity (which we here assume accounts for changes due to horizontal and vertical mixing), variations in nAT can be attributed to photosynthesis/respiration and the formation/dissolution of $CaCO_3$ since AT is insensitive to the air-sea exchange of CO_2. Computing potential alkalinity (pAT = AT + nitrate), following the definition of *Brewer and Goldman* [1976] allows the changes in AT due to the assimilation of nitrate and the release of inorganic nitrogen due to remineralization to be accounted for. These changes are small but allow the impact of photosynthesis (respiration) to be accounted for and changes due to carbonate mineral formation/dissolution to be elucidated [e.g., *Shadwick et al.*, 2014; *Roden et al.*, 2016] (Figure 7).

4. Discussion

4.1. Partitioning Seasonal TCO_2 Changes Across Physical and Biological Drivers

The seasonal TCO_2 deficits in both slope and shelf waters (Figure 1) were partitioned into the contributing physical and biological processes (Figure 8). While the total deficits of TCO_2 were of similar magnitude in the shelf and slope waters (Figure 8a), the contributions to the total seasonal change were distinct. The TCO_2 deficit in the slope waters is dominated by changes in salinity (Figure 8b); in this seasonally ice-covered region, the perennial formation and melt of sea ice exerts a dominant control on the regional hydrography, and subsequently the CO_2 system properties. By contrast, on the shelf, changing salinity accounted for less than half of the total TCO_2 deficit (Figure 8b). Biological processes (and gas exchange) made the largest contribution in the shelf waters, consistent with our observations of biological O_2 saturation (inferred from the O_2/Ar data) being elevated on the shelf (Figure 5d). In slope waters, areas of biological O_2 undersaturation were observed, potentially resulting from respiration or remineralization of organic
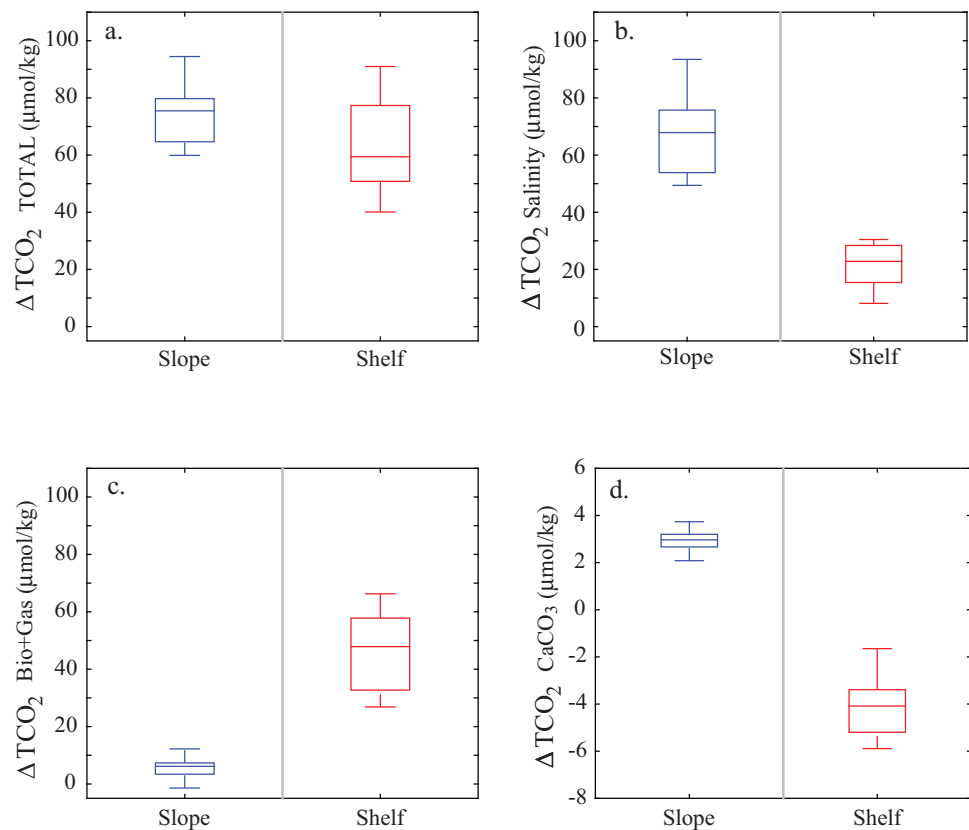

Figure 8. The (a) total deficit in surface TCO_2 in slope (blue, n = 10) and shelf (red, n = 12) waters and contributions from (b) salinity, (c) biology and gas exchange, and (d) carbonate mineral processes. Observations are from 2013.

matter, here reflected in the negative or near neutral contribution of the "bio + gas" term in the TCO_2 deficit on the slope.

The shelf waters were also distinct in terms of the contribution from $CaCO_3$ (inferred from the pAT, see Figure 7). On the shelf, we observed an elevated or excess nAT in the surface waters, reflecting a change in the ratio of TCO_2:AT consistent with the dissolution of $CaCO_3$. It has been shown that when brine is expelled from sea ice during formation, carbonate minerals may remain trapped in brine channels. The dissolution of these minerals may lead to an excess of AT within the ice that may be released to the surface waters during the spring and summer melt [*Rysgaard et al.*, 2007, 2009]. The release of excess AT to the surface waters may drive additional fCO_2 undersaturation, and elevated Ω and pH. However, our conventional salinity normalization assumes that sea ice melt water, the primary source of freshening in this system, makes a zero contribution to alkalinity, which may not be the case [e.g., *Jones et al.*, 2011].

To illustrate this point, we applied a normalization using a nonzero concentration of AT at zero salinity, here referred to as $AT_{residual}$; the value of $AT_{residual}$ was optimized to 700 μmol kg^{-1} for observations from the shelf stations by regression of AT and salinity data and estimated value of AT a salinity of zero. The surface waters no longer indicate an excess AT signal in the near surface waters when the residual AT is included in the normalization. Thus, it is possible that the meltwater influencing the (eastern) shelf stations has a residual alkalinity that is not accounted for with the traditional normalization. It is also likely that the residual alkalinity can vary with location, and so the freshwater input to the shelf stations differs from the freshwater input to the stations in the slope region further to the west.

Our observations on the shelf suggest that in addition to a biologically mediated fCO_2 undersaturation, there is a contribution from excess or residual AT in the surface waters, which may either be associated with $CaCO_3$ dissolution via the sea ice carbon pump, or the addition of meltwater with nonzero (residual) AT. Without an improved characterization of the AT (and TCO_2) in sea ice, neither process can be ruled out with the observations presented here, and while not negligible, these processes do make a small contribution to the overall change in TCO_2 (Figure 8d).

In the slope waters we observed a modest positive contribution of $CaCO_3$ to the total TCO_2 deficit. This would indicate the formation of $CaCO_3$ or a loss of AT. Previous work in this region has suggested that the waters in the slope region broadly indicate mixing between two end-members, with saline and CO_2-rich CDW (and mCDW) mixing with fresher, more CO_2 depleted waters that have been modified on the shelf [*Shadwick et al.*, 2014]. The 2:1 ratio between AT and TCO_2 in the slope waters has previously been attributed to formation and dissolution of $CaCO_3$ in the CDW rather than to local processes. While the southernmost stations on the slope had freezing, or near-freezing surface temperatures, these waters were also associated with negative values of O_2/Ar and undersaturated with respect to atmospheric CO_2, which would indicate the upward mixing of CDW rather than local precipitation of $CaCO_3$ via sea ice formation.

4.2. Interannual Variability in CO_2 System Properties

Observations from 2013 show that the surface waters on the Mertz shelf remain depleted in TCO_2 in the late-summer season, and mixed-layer TCO_2 concentrations were more similar to the post-MGT calving conditions of 2011 than the pre-MGT calving conditions of 2008 (see Table 1). Relatively fewer observations from 2012 also show surface TCO_2 depletion and enhanced carbonate saturation states (Ω roughly 2.1), with values exceeding the 2011 observations. In all three postcalving summers (2011, 2012, and 2013),

Table 1. Mixed-Layer Properties on the Shelf in 2008, 2011, 2012, and 2013[a]

	2008	2011	2012	2013
T	−1.01	−0.92	−1.02	−1.78
S	34.344	33.589	33.996	34.004
TCO_2	2170 (18)	2107 (20)	2109 (20)	2159 (25)
AT	2320 (15)	2280 (18)	2313 (15)	2315 (10)
Ω	1.51	1.9	2.1	1.7
pH	8.10	8.2	8.28	8.18

[a]Sampling occurred in January in 2008, 2011, and 2012, and in February 2013. Temperature (T) is in °C and salinity (S) is in kg m^{-3}. The number of stations sampled for CO_2 system properties was $n^{2008} = 47$; $n^{2011} = 45$; $n^{2012} = 9$; and $n^{2013} = 9$. The mean values of TCO_2 and TA (in μmol kg^{-1}, with standard deviation in parentheses) were used to compute the pH and saturation state, Ω.

mixed-layer depths were shallow relative to conditions in 2008, and to a lesser extent to observations in 2001 (see Table 1).

When comparing observations from the shelf between 2008 (pre-MGT calving) and 2011 (post-MGT calving), *Shadwick et al.* [2013a] reported an enhancement in surface saturation state and pH which was attributed to increased biological production. The mixed-layer TCO_2 depletion in 2011 was significantly enhanced relative to 2008. Furthermore, in the relatively lower salinity waters of the 2011 mixed layer, the biological enhancement of saturation state significantly outweighed the decrease due to dilution. This is in contrast to observations in the Arctic Ocean, which have linked sea ice meltwater with surface freshening and depressed saturation states [e.g., *Yamamoto-Kawai et al.*, 2009; *Mathis et al.*, 2011; *Yamamoto-Kawai et al.*, 2011], but in broad agreement with recent studies of coastal systems in the West Antarctic Peninsula region [*Hauri et al.*, 2015; *Jones et al.*, 2017]. If sea ice melt is associated with a source of dissolved iron (Fe) to the surface waters, this may stimulate biological productivity under otherwise Fe-limited conditions, which are common in the open Southern Ocean and occur seasonally in the marginal ice zone [e.g., *Sambrotto et al.*, 2003; *de Jong et al.*, 2013]. An increase in sea ice melt may therefore drive a localized negative feedback to ocean acidification in coastal Antarctic waters in the short term through fertilization of the surface waters [*Shadwick et al.*, 2013b].

While it may be possible to attribute the apparent continued enhancement in biological activity in the years following the MGT calving to changes in the physical system, or icescape, we note that the natural interannual variability in CO_2 system properties in this region, as in other coastal Antarctic settings [e.g., *Roden et al.*, 2013; *Legge et al.*, 2017], is likely to be large. However, an emerging understanding of the region indicates that the surface waters over the narrow continental shelf are biologically productive in the open water season and this appears to exert a dominant influence on the CO_2 system seasonality. The postcalving configuration of the polynya may favor enhanced surface TCO_2 depletions in the shelf waters, which is discussed in more detail below.

4.3. Interannual Variability in NCP

The productive season was well underway in January (2008, 2011, and 2012) and February (2013), inferred from remote sensing products that indicate elevated surface chlorophyll *a* concentrations in the months leading up to the period of observation. In 2008, 2011, and 2012, there is good agreement between the (independent) $nTCO_2$-based and $\Delta O_2/Ar$-based estimates of NCP (Table 2). Considering that the $nTCO_2$-based NCP integrates the mixed-layer carbon utilization from the beginning of the productive season, while the O_2/Ar method yields values from the preceding weeks only, the similarity between the two at the time of sampling in January suggests that the early spring production makes a relatively small contribution to seasonal NCP. The 2013 observations during February support this idea, since the $nTCO_2$-based estimates, which integrate over the spring and summer seasons and thus include contributions from the onset of production to February, are larger than the O_2/Ar-based estimates which reflect the lower productivity in February (Figure 9 and Table 2).

Observations in 2013 indicated daily rates of NCP from 30 to 80 mmol C m^{-2} d^{-1} associated mainly with waters over the continental shelf break, and net autotrophic conditions extending into February in waters east of the MGT (Figures 5d and 9). In the pre-MGT calving summer of 2008, the surface waters in the region indicated relatively homogenous distributions of modest biological oxygen supersaturation, and net autotrophic conditions with NCP on the order of 10 mmol C m^{-2} d^{-1} (Table 2). The maximum rates of NCP ($\sim$15 mmol C m^{-2} d^{-1}) were associated with the continental shelf break, at roughly 146°E (Figure 2b). In the first post-MGT calving summer of 2011 a region of very high NCP ($\sim$100 mmol C m^{-2} d^{-1}, Figure 9) was observed east of the former position of the MGT between 146°E and 148°E [*Shadwick et al.*, 2013a]. Daily rates of NCP were also large (30 and 80 mmol C m^{-2} d^{-1}) northwest of the

Table 2. Estimates of NCP (mmol C m^{-2} d^{-1}) in Shelf Waters Based on $nTCO_2$ Deficits (ΔTCO_2) and $\Delta O_2/Ar$[a]

Year (Month)	$nTCO_2$	$\Delta O_2/Ar$	MLD
2001 (Jan)	11–19		37
2008 (Jan)	13–27	9–15	61
2011 (Jan)	25–78	35–90	28
2012 (Jan)	35–76	45–90	25
2013 (Feb)	26–70	25–50	30

[a]The 2001 estimate is based on the nitrate deficit reported by *Sambrotto et al.* [2003] and converted to units of carbon using a ratio of C:N = 106:16.

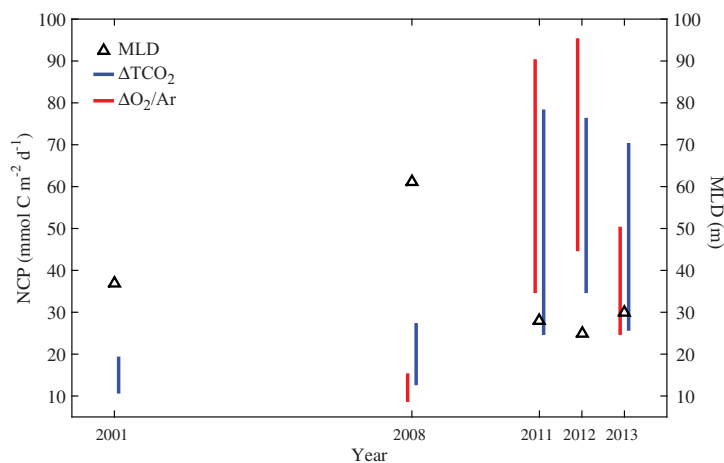**Figure 9.** Interannual variability in NCP over the shelf computed from $nTCO_2$ deficits (blue) and $\Delta O_2/Ar$ (red) between 2001 and 2013; variations in mixed-layer depth in black, see also Table 2.

grounded iceberg B09b in the vicinity of the Adélie depression (Figure 2c). In the second post-MGT calving summer of 2012, the highest rates of NCP ($\sim$100 mmol C m^{-2} d^{-1}) were observed just north of the Mertz Glacier Tongue (Figure 2c), and rates between 60 and 80 mmol C m^{-2} d^{-1}, Figure 9) were observed in waters over the continental shelf break, and in the region directly north of the fragments of iceberg B09b which had partially disintegrated (Figure 2d).

NCP was considerably lower in 2008 than 2011, 2012, and 2013, though of similar magnitude as in 2001. The mean postcalving rates of NCP estimated from seasonal $nTCO_2$ deficits is 47 mmol C m^{-2} d^{-1}, which suggests a more than two-fold increase relative to the mean precalving estimate, based on observations in 2001 and 2008 (Table 2) [*Sambrotto et al.*, 2003; *Shadwick et al.*, 2013a]. Particularly high rates of NCP were observed in 2011 and 2012 east of the former position of the MGT. As described above, in 2011, 2012, and 2013, elevated rates of NCP were observed south of roughly 66°S, in relatively shallow waters (<500 m) over the continental shelf, where the proximity to the sediments and the supply of melt water from the receding ice edge may supply iron to the surface waters and promote primary production [e.g., *Sambrotto et al.*, 2003; *de Jong et al.*, 2013].

The maximum rate of NCP in 2012 was 120 mmol C m^{-2} d^{-1}, near the edge of the MGT, and near the fragments of iceberg B9B, in both cases in the vicinity of small ice floes. Using a range of iron (Fe) to carbon ratios from 36 to 100 Fe:C [*de Baar et al.*, 2008] (Fe:C = μmol:mol), the amount of dissolved Fe needed to sustain the maximum observed NCP ranges from 4.3 to 12 μmol Fe m^{-2} d^{-1}. Applying an estimated flux of dissolved Fe from East Antarctic sea ice of 0.03–1.5 μmol Fe m^{-2} d^{-1} [*Lannuzel et al.*, 2007], the delivery of Fe from the sea ice would require a (daily) melt of $\sim$3 to 400 m^2 of ice. A large input of sea ice melt water in 2011 was reported by *Shadwick et al.* [2013a], and in the subsequent years, the absence of the MGT has likely allowed the westward drift of sea ice into the region. Thus, it is possible that the continued input of sea ice melt water in 2012 and 2013 contributed to the observed enhanced production through delivery of dissolved Fe and/or improved light conditions due to the shallow, fresh, mixed layer. While polynyas are thought to be regions of enhanced primary productivity due to the associated areas of open water, the overall reduction in the size of the Mertz Polynya has resulted in an increase in local NCP due to a reconfiguration of the icescape and possibly the additional input of macronutrients to the surface waters.

5. Conclusion

The dramatic changes to the physical environment or icescape in the Mertz Polynya precipitated by the movement of iceberg B09b and subsequent calving of the Mertz Glacier Tongue continue to influence the summer hydrography and biogeochemistry of the region 3 years later. The nearshore region east of Commonwealth Bay remains largely free of ice in the summer season and the narrow continental shelf is biologically productive and exhibits surface water undersaturation with respect to atmospheric CO_2. Late-summer observations in 2013 indicate that sea ice meltwater may provide a source of alkalinity, which contributes to the enhancement of carbonate saturation state and pH in the surface waters, which are also strongly influenced by organic matter production. Summer observations allow estimates of seasonal net community production to be made and yield an improved understanding of recent changes in the physical environment with respect to short-term biogeochemical impacts. The shelf waters to the east of Commonwealth Bay appear to have shifted towards enhanced surface carbonate saturation state and TCO_2 depletion largely

driven by biological processes which extend late into the summer season. Understanding the vulnerability of the system to future change, both natural (i.e., the growth and calving of the Mertz Glacier Tongue) and anthropogenic (i.e., increased atmospheric CO_2 and subsequent changes to the carbonate chemistry) change requires quantification of the drivers of variability outside of the productive season.

References

Arrigo, K. R., and G. L. van Dijken (2003), Phytoplankton dynamics within 37 Antarctic coastal polynya systems, *J. Geophys. Res.*, *108*(C8), 3271, doi:10.1029/2002JC001739.

Arrigo, K. R., and G. L. van Dijken (2004), Annual cycles of sea ice and phytoplankton in Cape Bathurst polynya, southeastern Beaufort Sea, Canadian Arctic, *Geophys. Res. Lett.*, *31*, L08304, doi:10.1029/2003GL018978.

Bates, N. R., D. A. Hansell, and C. A. Carlson (1998), Distribution of CO_2 species, estimates of net community production, and air-sea CO_2 exchange in the Ross Sea polynya, *Geophys. Res. Lett.*, *103*, 2883–2896.

Bender, M., J. Orchardo, M.-L. Dickson, R. Barber, and S. Lindley (1999), In vitro O_2 fluxes compared with ^{14}C production at other rate terms during the JGOFS Equatorial Pacific experiment, *Deep Sea Res., Part I*, *46*, 637–654.

Brewer, P. G., and J. C. Goldman (1976), Alkalinity changes generated by phytoplankton growth, *Limnol. Oceanogr.*, *21*, 108–117.

Cape, M. R., M. Vernet, M. Kahru, and G. Spreen (2014), Polynya dynamics drive primary production in the Larsen A and B embayments following ice shelf collapse, *J. Geophys. Res. Oceans*, *119*, 572–594, doi:10.1002/2013JC009441.

Cassar, N., M. L. Bender, B. A. Barnett, S. Fan, W. J. Moxim, H. Levy, and B. Tilbrook (2007), The Southern Ocean biological response to Aeolian iron deposition, *Science*, *317*, 1067–1070, doi:10.1126/science.1144602.

Cassar, N., B. A. Barnett, M. L. Bender, J. Kaiser, R. C. Hamme, and B. Tilbrook (2009), Continuous high-frequency dissolved O_2/Ar measurements by equilibrator inlet mass spectrometry, *Anal. Chem.*, *81*, 1855–1864, doi:10.1021/ac802300u.

Cassar, N., C. D. Nevison, and M. Manizza (2014), Correcting oceanic O_2/Ar-net community production estimates for vertical mixing using N_2O observations, *Geophys. Res. Lett.*, *41*, 8961–8970, doi:10.1002/2014GL062040.

Castro-Morales, K., N. D. R. Cassar Shoosmith, and J. Kaiser (2013), Biological production in the Bellingshausen Sea from oxygen-to-argon ratios and oxygen triple isotopes, *Biogeosciences*, *10*(4), 2273–2291, doi:10.5194/bg-10-2273-2013.

de Baar, H. J. W., L. J. A. Gerringa, P. Laan, and L. R. Timmermans (2008), Efficiency of carbon removal per added iron in ocean iron fertilization, *Mar. Ecol. Prog. Ser.*, *364*, 269–282.

de Jong, J., V. Schoemann, N. Maricq, N. Mattielli, P. Langhorne, T. Haskell, and J.-L. Tison (2013), Iron in land-fast sea ice of McMurdo Sound derived from sediment resuspension and wind-blown dust attributes to primary productivity in the Ross Sea, Antarctica, *J. Phycol.*, *38*, 844–861.

Dickson, A. G., and F. J. Millero (1987), A comparison of the equilibrium constants for the dissociation of carbonic acid in seawater media, *Deep Sea Res., Part II*, *34*, 1733–1743.

Dickson, A. G., C. L. Sabine, and J. R. Christian (Eds.) (2007), *Guide to Best Practices for Ocean CO_2 Measurement, PICES Spec. Publ. 3*, North Pacific Marine Science Organization, Sidney, B.C., Canada.

Dieckmann, G. S., G. Nehrke, S. Papadimitriou, J. Gottlicher, R. Steininger, H. Kennedy, D. Wolf-Gladrow, and D. N. Thomas (2008), Calcium carbonate as ikaite crystals in Antarctic sea ice, *Geophys. Res. Lett.*, *35*, L08501, doi:10.1029/2008GL033540.

Else, B., T. Papakyriakou, R. Galley, A. Mucci, M. Gosselin, L. Miller, E. Shadwick, and H. Thomas (2012), Annual cycles of pCO_2 in the southeastern Beaufort Sea: New understandings of air-sea CO_2 exchange in Arctic polynyas, *J. Geophys. Res.*, *117*, C00G13, doi:10.1029/2011JC007346.

Eveleth, R., M.-L. Timmermans, and N. Cassar (2014), Physical and biological controls on oxygen saturation variability in the upper Arctic Ocean, *J. Geophys. Res. Oceans*, *119*, 7420–7432, doi:10.1002/2014JC009816.

Geilfus, N.-X., G. Carnat, T. Papakyriakou, J.-L. Tison, B. Else, H. Thomas, E. H. Shadwick, and B. Dellile (2012), pCO_2 dynamics and related air-ice CO_2 fluxes in the Arctic coastal zone (Amundsen Gulf, Beaufort Sea), *J. Geophys. Res.*, *117*, C00G10, doi:10.1029/2011JC007118.

Grasshoff, K., K. Kremling, and M. Ehrhardt (Eds.) (2007), *Methods of Seawater Analysis*, 3rd ed., Wiley-VCH Verlag GmbH, Weinheim, Germany.

Hauri, C., S. C. Doney, T. Takahashi, M. Erickson, G. Jiang, and H. Ducklow (2015), Two decades of inorganic carbon dynamics along the West Antarctic Peninsula, *Biogeosciences*, *12*, 6761–6779, doi:10.5194/bg-12-6761-2015.

Ishii, M., H. Y. Inoue, and H. Matsueda (2002), Net community production in the marginal ice zone and its importance for the variability of the oceanic pCO_2 in the Southern Ocean south of Australia, *Deep Sea Res., Part II*, *49*, 1691–1706.

Jones, E. M., D. C. E. Bakker, H. J. Venables, M. J. Whitehouse, R. E. Korb, and A. J. Watson (2011), Rapid changes in surface water carbonate chemistry during Antarctic sea ice melt, *Tellus, Ser. B*, *62*, 621–635, doi:10.1111/j.1600-0889.2010.00496.x.

Jones, E. M., M. Fenton, M. P. Meredith, N. M. Clargo, S. Ossebaar, H. W. Ducklow, H. J. Venables, and H. J. de Baar (2017), Ocean acidification and calcium carbonate saturation states in the coastal zone of the West Antarctic Peninsula, *Deep Sea Res., Part II*, *139*, 181–194, doi:10.1016/j.dsr2.2017.01.007.

Kalnay, E., et al. (1996), The NCEP/NCAR 40-year reanalysis project, *Bull. Am. Meteorol. Soc.*, *77*, 437–471.

Körtzinger, A., et al. (2000), The international at-sea intercomparison of $f CO_2$ systems during the R/V Meteor Cruise 36/1 in the North Atlantic Ocean, *Mar. Chem.*, *72*, 171–192, doi:10.1016/S0304-4203(00)00080-3.

Lannuzel, D., V. Schoemann, J. deJong, J.-L. Tison, and L. Chou (2007), Distribution and biogeochemical behaviour of iron in the East Antarctic sea ice, *Mar. Chem.*, *106*, 18–32.

Laws, E. A. (1991), Photosynthetic quotients, new production and net community production in the open ocean, *Deep Sea Res., Part A*, *38*, 143–167.

Legge, O. J., D. C. Bakker, M. P. Meredith, H. J. Venables, P. J. Brown, E. M. Jones, and M. T. Johnson (2017), The seasonal cycle of carbonate system processes in Ryder Bay, West Antarctic Peninsula, *Deep Sea Res., Part II*, *139*, 167–180.

Lewis, E., and D. W. R. Wallace (1998), Program developed for CO_2 systems calculations, *Rep. ORNL/CDIAC 105*, Carbon Dioxide Inf. Anal. Cent., Oak Ridge Natl. Lab. U.S. Dep. of Energy, Oak Ridge, Tenn.

Massom, R. A., P. T. Harris, K. J. Michael, and M. J. Potter (1998), The distribution and formative processes of latent-heat polynyas in East Antarctica, *Ann. Glaciol.*, *27*, 420–426.

Mathis, J. T., J. N. Cross, and N. R. Bates (2011), Coupling primary production and terrestrial runoff to ocean acidification and carbonate mineral suppression in the eastern Bering Sea, *J. Geophys. Res.*, *116*, C02030, doi:10.1029/2010JC006453.

Mehrbach, C., C. H. Culberson, J. E. Hawley, and R. M. Pytkowicz (1973), Measurement of the apparent dissociation constants of carbonic acid in seawater at atmospheric pressure, *Limnol. Oceanogr.*, *18*, 897–907.

Miller, L. A., et al. (2002), Carbon distributions and fluxes in the North Water, 1988 and 1999, *Deep Sea Res., Part II*, *49*, 5151–5170.

Moreau, S., M. Vancoppenolle, L. Bopp, O. Aumont, G. Madec, B. Delille, J.-L. Tison, P.-Y. Barriat, and H. Goosse (2016), Assessment of the sea-ice carbon pump: Insights from a three-dimensional ocean-sea-ice biogeochemical model (NEMO-LIM-PISCES), *Elem. Sci. Anth.*, *4*, 122, doi:10.12952/journal.elementa.000122.

Mundy, C. J., and D. Barber (2001), On the relationship between spatial patterns of sea-ice tip and the mechanisms which create and maintain the North Water (NOW) Polynya, *Atmos. Ocean*, *39*, 327–341.

Nihashi, S., and K. I. Ohshima (2015), Circumpolar mapping of Antarctic coastal polynyas and landfast sea ice: Relationship and variability, *J. Clim.*, *28*, 3650–3670.

Ohshima, K. I., S. Nihashi, and K. Iwamoto (2016), Global view of sea-ice production in polynyas and its linkage to dense/bottom water formation, *Geosci. Lett.*, *3*, 13, doi:10.1186/s40562-016-0045-4.

Orsi, A. H., G. C. Johnson, and J. L. Bullister (1999), Circulation, mixing, and production of Antarctic Bottom Water, *Prog. Oceanogr.*, *43*, 55–109.

Pierrot, D., C. Neill, K. Sullivan, R. Castle, R. Wanninkhof, H. Lüger, T. Johannessen, A. Olsen, and R. A. Feely (2009), Recommendations for autonomous underway pCO_2 measuring systems and data reduction routines, *Deep Sea Res., Part II*, *56*, 512–522, doi:10.1016/j.dsr2.2008.12.005.

Reuer, M. K., B. A. Barnett, M. L. Bender, P. G. Falkowski, and M. B. Hendricks (2007), New estimates of Southern Ocean biological production rates from O_2/Ar ratios and the triple isotope composition of O_2, *Deep Sea Res., Part I*, *54*, 951–974.

Riley, J. P., and M. Tongudai (1967), The major cation/chlorinity ratios in sea water, *Chem. Geol.*, *2*, 263–269.

Rintoul, S. R. (1998), On the origin and influence of Adlie Land Bottom Water, in ocean, ice, and atmosphere: Interactions at the Antarctic continental margin, *Antarct. Res. Ser.*, *75*, 151–171.

Roden, N. P., E. H. Shadwick, B. Tilbrook, and T. W. Trull (2013), Annual cycle of carbonate chemistry and decadal change in coastal Prydz Bay, East Antarctica, *Mar. Chem.*, *155*, 135–147.

Roden, N. P., B. Tilbrook, T. W. Trull, P. Virtue, and G. D. Williams (2016), Carbon cycling dynamics in the seasonal sea-ice zone of East Antarctica, *J. Geophys. Res. Oceans*, *121*, 8749–8769, doi:10.1002/2016JC012008.

Rosenberg, M., and S. Rintoul (2010), *Aurora Australis Marine Science Cruises AU0803 and AU0806: Oceanographic Field Measurements and Analysis*, Antarct. Clim. and Ecosyst. Coop. Res. Cent., Hobart, Australia.

Rosenberg, M., and S. Rintoul (2011), *Aurora Australis Marine Science Cruises AU1121: Oceanographic Field Measurements and Analysis*, Antarct. Clim. and Ecosyst. Coop. Res. Cent., Hobart, Australia.

Rosenberg, M., and S. Rintoul (2012), *Aurora Australis Marine Science Cruises AU1203: Oceanographic Field Measurements and Analysis*, Antarct. Clim. and Ecosyst. Coop. Res. Cent., Hobart, Australia.

Rysgaard, S., R. N. Glud, M. K. Sejr, J. Bendtsen, and P. B. Christensen (2007), Inorganic carbon transport during sea ice growth and decay: A carbon pump in polar seas, *J. Geophys. Res.*, *112*, C03016, doi:10.1029/2006JC003572.

Rysgaard, S., J. Bendtsen, L. T. Pedersen, H. Ramlov, and R. N. Glud (2009), Increased CO_2 uptake due to sea ice growth and decay in the Nordic Seas, *J. Geophys. Res.*, *114*, C09011, doi:10.1029/2008JC005088.

Sambrotto, R. N., A. Matsuda, R. Vaillancourt, M. Brown, C. Langdon, S. S. Jacobs, and C. Measures (2003), Summer plankton production and nutrient consumption patterns in the Mertz Glacier Region of East Antarctica, *Deep Sea Res., Part II*, *50*, 1393–1414, doi:10.1016/S0967-0645(03)00076-6.

Shadwick, E. H., H. Thomas, M. Chierici, B. Else, A. Fransson, C. Michel, L. A. M. A. Mucci, A. Niemi, T. N. Papakyriakou, and J.-E. Tremblay (2011), Seasonal variability of the inorganic carbon system in the Amundsen Gulf region of the southeastern Beaufort Sea, *Limnol. Oceanogr.*, *56*(1), 303–322.

Shadwick, E. H., S. R. Rintoul, B. Tilbrook, G. D. Williams, N. Young, A. D. Fraser, H. Marchant, J. Smith, and T. Tamura (2013a), Glacier tongue calving reduced dense water formation and enhanced carbon uptake, *Geophys. Res. Lett.*, *40*, 904–909, doi:10.1002/grl.50178.

Shadwick, E. H., T. W. Trull, H. Thomas, and J. A. E. Gibson (2013b), Vulnerability of polar oceans to anthropogenic acidification: Comparison of Arctic and Antarctic seasonal cycles, *Nat. Sci. Rep.*, *3*, 2339, doi:10.1038/srep.02339.

Shadwick, E. H., B. Tilbrook, and G. D. Williams (2014), Carbonate chemistry in the Mertz Polynya (East Antarctica): Biological and physical modification of dense water outflows and the export of anthropogenic CO_2, *J. Geophys. Res. Oceans*, *119*, 1–14, doi:10.1029/2013JC009286.

Shadwick, E. H., B. Tilbrook, N. Cassar, T. W. Trull, and S. R. Rintoul (2015), Summertime physical and biological controls on O_2 and CO_2 in the Australian Sector of the Southern Ocean, *J. Mar. Syst.*, *147*, 21–28, doi:10.1016/j.jmarsys.2013.12.008.

Smith, W. O., and L. O. Gordon (1997), Hyperproductivity of the Ross Sea (Antarctica) polynya during austral spring, *Geophys. Res. Lett.*, *24*, 233–236.

Sweeney, C., et al. (2000), Nutrient and carbon removal ratios and fluxes in the Ross Sea, Antarctica, *Deep Sea Res., Part II*, *47*, 3395–3421.

Tamura, T., K. I. Ohshima, and S. Nihashi (2008), Mapping of sea ice production for Antarctic coastal polynyas, *Geophys. Res. Lett.*, *135*, L07606, doi:10.1029/2007GL032903.

Tamura, T., G. D. Williams, A. D. Fraser, and K. I. Ohshima (2012), Potential regime shift in decreased sea ice production after the Mertz Glacier calving, *Nat. Commun.*, *3*, 826, doi:10.1038/ncomms1820.

Wanninkhof, R. (2014), Relationships between wind speed and gas exchange over the ocean revisited, *Limnol. Oceanogr. Methods*, *12*, 351–362, doi:10.4319/lom.2014.12.351.

Weiss, R. F. (1974), Carbon dioxide in water and seawater: The solubility of a non-ideal gas, *Mar. Chem.*, *2*, 203–215.

Williams, G. D., and N. L. Bindoff (2003), Wintertime oceanography of the Adélie Depression, *Deep Sea Res., Part II*, *50*, 1373–1392.

Williams, M. (2013), *RV Tangaroa Voyage Report Tan1302? Mertz Polynya Voyage*, Natl. Inst. of Water and Atmos. Res., Wellington.

Yager, P. L., D. W. R. Wallace, K. M. Johnson, W. O. Smith, P. J. Minnett, and J. W. Deming (1995), The Northeast Water Polynya as an atmospheric CO_2 sink: A seasonal rectification hypothesis, *J. Geophys. Res.*, *100*, 4389–4398.

Yamamoto-Kawai, M., F. A. McLaughlin, E. C. Carmack, S. Nishino, and K. Shimada (2009), Aragonite undersaturation in the Arctic Ocean: Effects of ocean acidification and sea ice melt, *Science*, *326*, 1098–1100, doi:10.1126/science.1174190.

Yamamoto-Kawai, M., F. A. McLaughlin, and E. C. Carmack (2011), Effects of ocean acidification, warming and melting of sea ice on aragonite saturation of the Canada Basin surface water, *Geophys. Res. Lett.*, *38*, L03601, doi:10.1029/2010GL045501.

Young, N., B. Legrésy, R. Coleman, and R. Massom (2010), Mertz Glacier Tongue unhinged by giant iceberg, *Aust. Antarct. Mag.*, *18*, 19.